NEURAL NETWORK APPROACH TO DIAGNOS OF CORONARY ARTERY DISEASE IN NUCLEAR MEDICINE

H. Bagher-Ebadian,[1,2,3] *H. Soltanian-Zadeh,*[3,4] *S. Setayeshi*[1]

[1] Department of Physics, Amir-Kabir University of Technology, Tehran, Iran
[2] Research Institute of Nuclear Medicine, Shariati Hospital, Tehran, Iran
[3] Radiology Image Analysis Lab, Henry Ford Health System, Detroit, MI 48202, USA
[4] Department of Electrical and Computer Engineering, Tehran University, Tehran 14399, Iran

ABSTRACT

We developed a neural network to predict coronary artery disease (CAD) from planar images in nuclear medicine. The proposed method can aid to diagnose coronary artery disease in 99Tc-sestamibi myocardial imaging. Classification of myocardium from its background was done by fuzzy clustering using Picard iteration algorithm. A back-propagation artificial neural network (ANN) classifier was trained and tested with leave-one-out method. The patient population included 58 subjects (30 male, 28 female). Scintigraphy images were obtained in stress and rest phases and after perfusion study, patients also had angiography. Our gold standard was the results of coronary angiograms in acute phase. The performance of the optimal ANN was analyzed by receiver operating characteristic (ROC) methodology. The result of ANN, compared with the nuclear medicine ward and two physicians using the ROC method, shows that the proposed method outperforms visual diagnosis and is useful for CAD diagnosis from planar images in nuclear medicine.

1. INTRODUCTION

Visual interpretation of images in nuclear medicine, even by experienced observers, is subject to substantial variability [1]. The Tc^{99m}-sestamibi myocardial SPECT imaging has been reported to offer major improvements over planar imaging in the diagnosis of coronary artery disease [2]. Even with this technique, many problems have been indicated. In addition, the number of experienced radiologists in this field is limited. The development of a computer-aided diagnostic system or expert system is considered helpful for diagnosis of coronary artery disease (CAD) in nuclear medicine [3]. An expert system (PERFEX) developed for the computer-assisted interpretation of myocardial perfusion SPECT studies is now available. However, a systematic validation of the diagnostic performance of this expert system for the interpretation of myocardial perfusion SPECT studies has not been reported [4]. PERFEX uses the certainty of the location, size, shape and reversibility of the perfusion defects based on polar maps and angiography to infer the certainty of the presence and location of CAD [4].

The purpose of this study is to develop a computerized system using fuzzy clustering and neural networks, which can aid physicians and radiologists in the diagnosis of coronary artery disease and interpretation of planar images for CAD. We have segmented the myocardium from its background using fuzzy clustering with a Picard iteration algorithm. Then we applied a neural network for CAD diagnosis. The performance of network was compared to interpretation of two expert physicians and nuclear medicine ward, using coronary angiography as gold standard [5].

2. MATERIAL AND METHODS

2.1. Data Collection

The total study population consisted of 58 patients (30 male, 28 female). Patients, who had undergone both rest-stress myocardial perfusion planar scan and coronary angiography were studied retrospectively. The interval between perfusion study and angiography was below the 3 months (acute time). As shown in Table I and according to the results of patients angiograms, there were thirty-three abnormal and twenty-five normal subjects. The scintigraphy image data were acquired in planar method for three projections (Anterior, Left Anterior Oblique -45 and Left Lateral) with a $400mm$ gamma camera circular crystal, using a low-energy, general-purpose collimator (FWHM 8.4mm at 15cm) and a zoom factor 1.46 (pixel size 5.45 mm). The size of each image was 64×64. For each patient, the images were acquired in two phases (rest and stress). Operator used a lead tray to omit the effect of liver superposition. Rest and stress studies were performed in a

2-day Tc^{99m}- Sestamibi Bruce protocol, using 740 MBq at stress and, after 24 hr, 740 MBq at rest.

2.2. Image Segmentation

The noise of myocardium background, was suppressed by segmenting of myocardium form its background. In this study, images were segmented by fuzzy clustering using Picard iteration algorithm [6]. Each projection was segmented in three stages and in each stage, Picard iteration algorithm was used for Bi-Modal fuzzy clustering. At first, initialization of membership values was random, but in the subsequent stages, the memberships were filled by previous values in order to expedite the convergence. Euclidian distance was used as the distance metric in Picard iteration algorithm and the normalized count in each projection was used for histogram generation.

2.3. Feature Extraction

The location of vessels in myocardium varies from patient to patient. Regarding to the nature of cardiac planar images and the number of projections obtained, the myocardium was partitioned into four regions. As shown in Fig. 1, the center of activities (*ox*,*oy*) was calculated for each segmented projection using the following Eq. (1) and Eq. (2).

$$oy = \overline{Y} = \frac{m_{01}(R_0)}{m_{00}(R_0)} \quad , \quad ox = \overline{X} = \frac{m_{10}(R_0)}{m_{00}(R_0)} \tag{1}$$

$$m_{pq}(R) = \iint_R f(x,y)(x-\overline{X})^p (y-\overline{Y})^q \, dxdy \tag{2}$$

Circumferential profiles around the center of activity were calculated for each projection. For all projections, the size of radii was fixed to epicardial variation detection. As shown in Fig. 1, direction of sampling was clockwise and the angle interval of each region was 90 degrees. The centers of polar transform for three projections have been shown in Fig. 1. The six transformed projections (three stress and three rest) are shown in Fig. 2. Two feature vectors were extracted from stress and rest phases of each patient. As shown in Fig. 2, each phase consists of twelve regions and therefore, feature vectors dimension is twelve. According to Eq. (3) and Eq. (4), we consider the mean and variance row vectors as our feature vectors. As shown in Eq. (3), $\vec{\mu}_p = [\mu_p^1, \mu_p^2, \mu_p^3 ... \mu_p^{12}]$ denotes the mean vector obtained from phase *p* (stress or rest). The $\vec{H}_p(i,j)$ points out to the amount of count in position *(i,j)* in polar image for phase *p*. The $\vec{A}_p$, was obtained by Eq. (5) in which $\bar{I}_p(i,j)$ was defined by Eq. (6). The CAD was detected by variation of activities between rest and stress phases for all

$$\mu_p^m = \frac{1}{A_p^m} \sum_i \sum_j H_p^m(i,j) \ , \qquad 1 \le m \le 12 \tag{3}$$

$$\Sigma_p^m = \frac{1}{A_p^m} \sum_i \sum_j [H_p^m(i,j) - \mu_p^m]^2 \ , \qquad 1 \le m \le 12 \tag{4}$$

$$A_p^m = \sum_i \sum_j I_p^m(i,j) \tag{5}$$

$$I_p^m(i,j) = \begin{cases} 1, & H_p^m(i,j) \neq 0 \\ 0, & H_p^m(i,j) = 0 \end{cases} \tag{6}$$

three projections. For this reason, we introduced the following feature vectors.

$$\Delta\vec{\mu} = \vec{\mu}_{\mathrm{Re}\,st} - \vec{\mu}_{Stress} \tag{7}$$

$$\Delta\vec{\Sigma} = \vec{\Sigma}_{\mathrm{Re}\,st} - \vec{\Sigma}_{Stress} \tag{8}$$

Each feature vector ($\Delta\vec{\mu}$ or $\Delta\vec{\Sigma}$) consists of twelve elements. For all patients, these feature vectors were extracted from projections and the best features were selected using the maximization of feature distances in feature space. The result of maximization showed that the optimal feature vector was the difference vector between the mean vectors obtained at stress and rest, i.e., $\vec{\mu}_p = [\mu_p^1, \mu_p^2, \mu_p^3 ..... \mu_p^{12}]$.

2.4. Artificial Neural Network

We used a feed-forward back-propagation ANN for feature classification in the selected feature space (differences of means). We applied a leave-one-out method for training, testing and ANN classifier optimization. In the present study, all images of the same patient were left out as test samples in each training cycle and the images from the other (N-1) patients were used for training. The results of all test images from the N training cycles were accumulated to form a test score distribution or correct classification fraction (CCF). This fraction is computed as the ratio of successful classification by the ANN to the total number of samples. The number of hidden layer nodes may affect the performance of the ANN classifier [7]. The performance of ANN with respect to the number of hidden layer nodes was examined by considering the ANN responses at the preset ANN training termination error level (error = 0.32). Finally, The performance of the optimal ANN classifier was evaluated by ROC methodology. The output value of the ANN was used as the decision variable in the ROC analysis. An ROC curve, which is the relationship between the true-positive fraction (TPF) and false-positive fraction (FPF), is generated by setting different decision thresholds on the output values of the ANN at preset training termination error level (error = 0.32). The performance of the optimal

ANN was determined by *Az* test, which is the area under the ROC curve.

3. EXPERIMENTAL RESULTS

Fig. 3 shows the typical variation of the total sum square error for ANN as the number of epoches is increased. In this example, data are presented for the ANN with 13:5:1 architecture (optimal). A typical cumulative score for correct classification fraction (CCF) shown in Fig. 4, indicates that the CCF increases as the number of epoches is increased. The training and optimization were repeated for the ANN with different nodes in the hidden layer. In each case, the final CCF at the termination error level (error level = 0.32) was determined [7]. The ANN structure with maximum CCF value was considered as the optimal network. As shown in Fig. 5, the optimal number of nodes in the hidden layer was five (CCF value = 0.74). Then the ROC curve was generated for this optimal architecture (13:5:1) has shown in Fig. 6. The results obtained from two physicians and the nuclear medicine ward at shariati hospital, Tehran, Iran are also shown in Fig. 6. The overall performance of the optimal ANN (13:5:1, error = 0.32) was determined as the integral under the ROC curve, which was 0.80. Amounts of positive predictive value (PPV) and negative predictive value (NPV) at the prevalence of 0.54 were also estimated for the population. In addition, NPV and PPV for an optimal threshold, which is found as the intersection of the ROC curve with the line of Sensitivity = Specificity were computed. Table II compares the values of PPV and NPV for the two physicians, the nuclear medicine ward, and the ANN. This Table clearly illustrates superiority of the ANN compared to the visual inspection of the results by the physicians.

4. DISCUSSION

Our attempt to apply neural network for CAD detection in nuclear medicine has been quite successful in acute phase of myocardial infarction. The ANN proved to be capable of extracting essential characteristics from noisy images and learning from angiograms. The recognition performance of the optimal ANN is superior to that of the experienced physicians (see Fig. 6 and Table II). As shown in Table II, the ANN detects CAD in myocardial planar images more accurately than the expert physicians and nuclear medicine ward.

Determining the amount and location of coronary artery stenosis, clearly needs more clinical and technical information. Limited accuracy of coronary angiography and myocardial SPECT for predicting the site of subsequent acute MI (myocardium infarction) are reported by some researchers [8]. Correlation between the location of a SPECT defect, the most severe coronary stenosis, and the location of a subsequent AMI (acute myocardium infarction) and concordance between SPECT and coronary angiography to identify the most severe defects are investigated by other researchers [9]. However, considering the results presented in the literature, it can be concluded that prediction of disease (CAD) versus no-disease (no-CAD) from the perfusion study is more reliable than prediction of CAD location, site and amount of stenosis. Therefore, our task was prediction of CAD in acute time for mild, moderate, and severe cases from planar perfusion images.

The SPECT images are constructed from series of planar images with major properties of LV-orientation and liver superposition. It is impossible to omit the effect of liver superposition from the SPECT images during the data acquisition and the LV-orientation may vary from patient to patient. The proposed method relies on the operator for detecting the LV orientation and omitting the liver superposition in six spot views. This method may be applied to SPECT images using three spot views (ANT, LAO45, Lt. LAT) from series of images in each phase and liver patterns may be separated from each spot by manual or semi-automated methods. The six spot views should be selected based on LV-orientation using manual or semi-automated methods. Sets of the six views in the rest and stress can be used as the input of the proposed method for pre-diagnosis of CAD.

Accurate determination of the location and amount of the disease using the techniques developed in this paper may be considered as a direction for future work. Another direction can be finding of the optimal set of myocardium segments, which are more sensitive compared to the other sets for detection of CAD. This optimization can be done for offset location and number of myocardium segments.

TABLE I

Patient population and diagnosis of physicians ward (Positive or Negative) regarding their angiograms.

	TP	TN	FP	FN
Male	10	6	8	6
Female	12	4	7	5
Total	22	10	15	11

TABLE II

Positive prediction values and negative prediction values for nuclear medicine ward, expert #1 and #2 at prevalence of 0.568 corresponding specificities and sensitivities.

	SPC	SEN	PPV	NPV
WARD	0.40	0.66	59%	60%
ANN – WARD	0.40	0.92	67%	80%
EXPERT#1	0.20	0.75	55%	70%
ANN-EXPERT#1	0.20	0.97	52%	84%
EXPERT#2	0.32	0.60	54%	53%
ANN-EXPERT#2	0.32	0.95	65%	83%
ANN-OPTIMUM	0.73	0.72	80%	68%

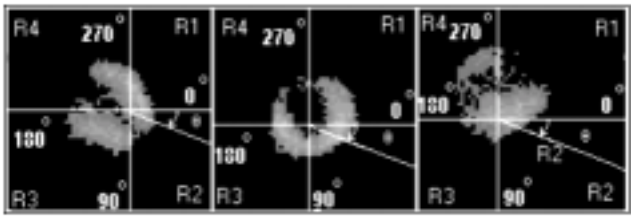

Figure 1. Four regions with respect to their center of activity after fuzzy clustering segmentation.

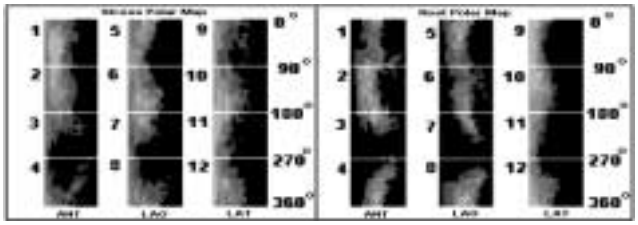

Figure2. Six projections after polar map transformation.

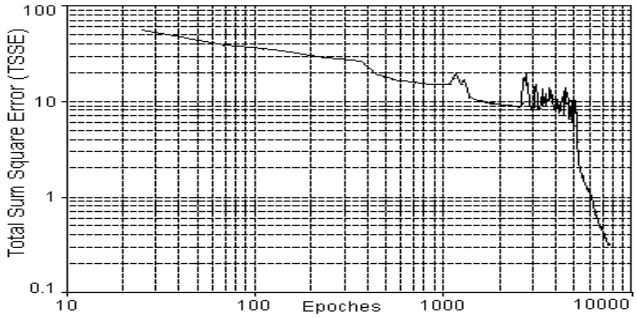

Figure 3. Total Sum Square Error Versus Epoches (13:5:1).

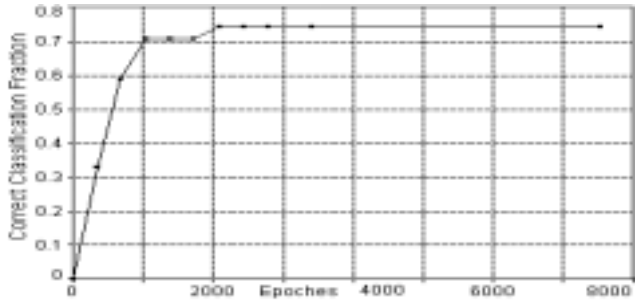

Figure 4. Correct Classification Fraction Versus Epoches for Optimal ANN (13:5:1)

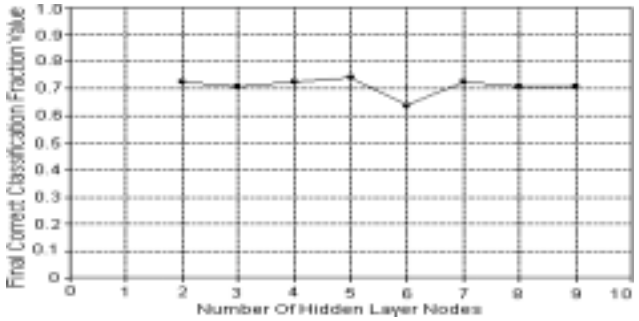

Figure 5. Hidden Layer Node Optimization Using Final Correct Classification Value.

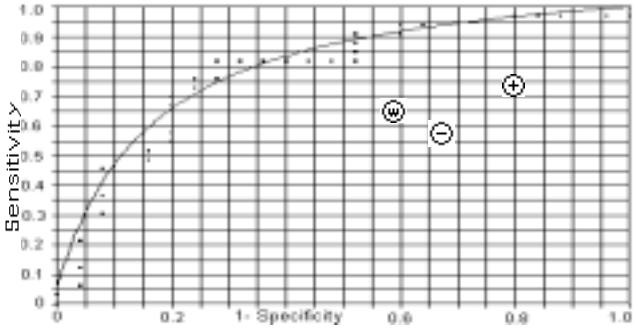

Figure 6. Receiver Operator Characteristic curve for the optimal ANN, with points representing the physician's performance.

Ⓦ Nuclear Medicine Ward: TPF: 0.66, FPF: 0.60
⊕ Expert (Physicien) No.1: TPF: 0.75, FPF: 0.80
⊖ Expert (Physicien) No.2: TPF: 0.60, FPF: 0.68

5. REFERENCES

[1] G.B. Trobaugh, F.J.T. Wackeres, E.B. Sokole, T.A. Derouen, J.L. Ritchi, G.W. Hamilton: "Thallium-201 Myocardial Imaging: An Interinstitial Study of Observer Variability," *Journal of Nuclear Medicine*, Vol. 19, pp. 359-363, 1978.

[2] M.J. Guiberteau: "Nuclear Cardiovascular Imaging: Current Clinical Practice," New York: *Churchill Livingston*, 1990.

[3] F. Hiroshi, K. Tetsuro: "Neural Network Approach for Computer-Aided Diagnosis of Coronary Artery Diseases in Nuclear Medicine," *IEEE Transaction on Nuclear Science*, pp. III-215-III-220, 1992.

[4] E.V. Garcia, C.D. Cooke, R.D. Folks, C.A. Santana, E.G. De, L. Braal, N.F. Ezquerra: "Diagnostic Performance of an Expert System for the Interpretation of Myocardial Perfusion SPECT Studies," *Journals of Nuclear Medicine*, Vol. 42, No. 8, pp. 1185-1191, 2001.

[5] J. Krzysztof, S. Lucy, K. Kanu, S. Gursel: "A Novel Algorithm for Classification of SPECT Images of a Human Heart," *Ninth IEEE Symposium on Computer-Based Medical Systems*, Vol. 1, p. 1-5, 1996.

[6] C.V. Jawahar and P.K. Biswas: "Investigation on Fuzzy Thresholding Based on Fuzzy Clustering," *Pattern Recognition*, Vol. 41, No. 10, pp. 1605-1613, 1997.

[7] M.E. Ashrafi, H. Bagher-Ebadian, E. Yahaghi: "Pre-Optimization of Radiotherapy Treatment Planning: An Artificial Neural Network Calssification Aided Technique," *Physics in Medicine and Biology*, Vol. 44, Issue 6, pp. 1513-1528, June 1999.

[8] W.C. Little, M. Constantinescu, R.J. Applegate " Can Coronary Angiography Predict the Site of a Subsequent Myocardial Infarction in Patients with Mild-to-Moderate Coronary Artery Disease*?*," *Circulation*, Vol. 78, p. 1157-1166, 1988.

[9] J. Candell-Riera, O. Pereztol-Valdes, C. Santana-Boado, M. Missorici, G. Oller-Martinez, S. Aguade-Bruix, J. Castell-Conesa, M. Simo, M.J. Diez-Castro and J. Soler-Soler " Relationship Between the Location of the Most Severe Myocardial Perfusion Defects, the Most Severe Coronary Artery Stenosis, and the Site of Subsequent Myocardial Infarction," *Journals of Nuclear Medicine*, Vol. 42, No. 4, p. 558-563, April 2001.